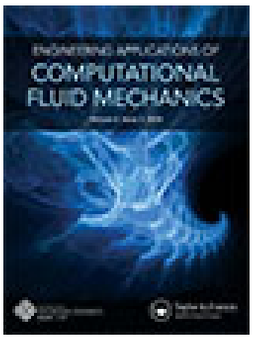

Engineering Applications of Computational Fluid Mechanics

ISSN: 1994-2060 (Print) 1997-003X (Online) Journal homepage: www.tandfonline.com/journals/tcfm20

LBM Simulation of a Droplet Dripping Down a Hole

R. Haghani, M. H. Rahimian & M. Taghilou

To cite this article: R. Haghani, M. H. Rahimian & M. Taghilou (2013) LBM Simulation of a Droplet Dripping Down a Hole, Engineering Applications of Computational Fluid Mechanics, 7:4, 461-470, DOI: 10.1080/19942060.2013.11015485

To link to this article: https://doi.org/10.1080/19942060.2013.11015485

Published online: 19 Nov 2014.

Submit your article to this journal

Article views: 771

View related articles

Full Terms & Conditions of access and use can be found at
https://www.tandfonline.com/action/journalInformation?journalCode=tcfm20

Engineering Applications of Computational Fluid Mechanics Vol. 7, No. 4, pp. 461–470 (2013)

LBM SIMULATION OF A DROPLET DRIPPING DOWN A HOLE

R. Haghani *, M. H. Rahimian *† and M. Taghilou**

* *School of the Mechanical Engineering, College of Engineering University of Tehran, Tehran Iran*
† *E-Mail: rahimyan@ut.ac.ir* (*Corresponding Author*)
** *Faculty of Mechanical Engineering, University of Tabriz, Tabriz, Iran*

ABSTRACT: A droplet dripping through a hole, which is located on a horizontal plate, was simulated in the current work. To overcome the numerical instabilities and accommodate the high density and viscosity ratios, Lee's LBM model was used to simulate the two-phase flow. Also wettability effect was taken into account by imposing the contact angle between solid-liquid and gas phases using Cahn's wetting theory. The effects of gravitational acceleration, surface tension, equilibrium contact angle, viscosity ratio, density ratio, and also the geometrical parameters, such as the height and width of the hole, have been investigated separately. In addition to numerical results, high numerical stability and ease of using surface tension and contact angle for controlling fascinated the authors to model this problem. High numerical stability in capturing the remaining fine particles on the surface and slender strip of a droplet passing through a small hole is a significant contribution. The results show that gravitational force and adhesion force caused by surface tension, are opposing forces influencing droplet behaviour. Enhancing the contact angle to more than 90 degrees makes the surface hydrophobic and the droplet will drip under gravitational force. Also increasing the surface tension causes increasing adhesion force, which leads to droplet decay. In this case some parts of the droplet will remain on the surface.

Keywords: lattice Boltzmann, droplet, contact angle, Archimedes, Ohnesorge

1. INTRODUCTION

Two-phase flow investigation with consideration of the wettability effect has been conducted by several authors. An understanding of the effect relies on the vast applied and theoretical background of two-phase studies. Any increase in the quality of inkjet printers depends directly on the droplet radius after impingement and its spreading rate. Also cooling processes may be considerably affected by the dripping or impacting of a cold droplet on the hot surface. Experimental and numerical study about the impact of a droplet on a layer of the same liquid on a solid surface was presented by Pan and Law (2007). There are also some experimental studies which have been done in order to investigate the impact of droplets on a thin film layer (Cossali et al., 2004; Wal et al., 2006; Castanet et al., 2009). Krause et al. (2011) simulated droplet formation and interaction in emulsification processes. They introduced a modified standard Volume of Fluid model (VOF), which allows droplet interactions on the macroscale including droplet contact, coalescence or bouncing. Lunkad et al. (2007) applied the volume of fluid (VOF) method to study the droplet dynamics, impacting the horizontal and sloping surfaces. Manservisi and Scardovelli (2009) suggested a new approach based on finite element which is coupled with a front-tracking method for predicting the droplet behaviour on horizontal surface with different wettabilities. In all these traditional approaches, Lattice Boltzmann Method (LBM) has been applied as an efficient scheme to two-phase flow modelling. Some early efforts could be found in this direction (Chen and Doolen, 1998; Succi, 2001). Lately Inamuro et al. (2004) suggested a model using Diffuse Interface Method (DIM) in LBM framework, considering two-phase flow with density ratios over 1000. Yoshino and Mizutani (2006) implemented this model using wetting potential boundary conditions suggested by Briant et al. (2002 and 2004) to consider the contact angle effect. Ghosh et al. (2012) investigated numerically bubble dynamics in an inclined water column. They proposed a 3D LBM which handles diffuse interface concepts. Recently, Lee (2009) proposed a novel model which utilizes the pressure equation to consider the incompressibility. His method can simulate two-phase flow in wide ranges of density and viscosity ratios (up to 1000). In this model, spurious velocities at the interface have been totally eliminated. This point has been considered as a significant achievement (Connington and Lee, 2012; Kupershtokh et al., 2009) because existence of parasitic velocities at the interface, besides causing the defect on reaching the true equilibrium condition, can debilitate the model

Received: 19 Mar. 2013; Revised: 9 Jul. 2013; Accepted: 15 Jul. 2013

capability in wide range of variable changes. This fact is highlighted when the characteristic velocity of the problem is in low range. In order to simulate the contact angle effect Lee and Liu (2005) developed Lee's method using Cahn-Hilliard diffuse interface theory. Taghilou and Rahimian (2012) investigated two-phase flow inside porous media via Lee's method. They simulated droplet dynamics inside artificial porous media and investigated flow characteristic parameters on the droplet behaviour.

In the current work, Lee's LBM method is used to simulate the sneaking motion of a droplet through a vertical hole under the influence of gravity, surface tension and wettability effect, which can be seen in the refinery and petrochemical reactors. High numerical stability in capturing the remaining fine particles on the surface and slender strip of a droplet passing through a small hole is a significant contribution of this work. The effects of parameters, such as equilibrium contact angle and height and width of the hole are discussed. The influence of gravitational acceleration measured by Archimedes number and Ohnesorge number expresses the effect of surface tension. Also equilibrium contact angle behaviour has been studied. The relation between the droplet and the surface is divided into four categories, the balance of the droplet on the top surface, the balance of the droplet on the bottom surface and decay and dripping of the droplet.

2. GOVERNING EQUATIONS

2.1 Two-phase modeling

Boltzmann equation in discrete form for the mass transfer and momentum equations for a system consisting of two non-compressible fluids can be written as follows (He et al., 1998):

$$\frac{\partial f_\alpha}{\partial t}+\mathbf{e}_\alpha.\nabla f_a=-\frac{1}{\lambda}\left(f_\alpha-f_\alpha^{eq}\right)+\frac{1}{\rho c_s^2}(\mathbf{e}_\alpha-\mathbf{u}).\mathbf{F}f_\alpha^{eq} \quad (1)$$

In the above equation f_α stands for the distribution function for the particles, which have discrete velocities indicated by $\mathbf{e}_\alpha$, $\mathbf{u}$ expresses the macroscopic velocity, c_s corresponds to the sound speed, λ is related to relaxation time and f_α^{eq} indicates the equilibrium distribution function as follows.

$$f_\alpha^{eq}=w_\alpha\rho[1+\frac{\mathbf{e}_\alpha.\mathbf{u}}{c_s^2}+\frac{(\mathbf{e}_\alpha.\mathbf{u})^2}{2c_s^4}-\frac{(\mathbf{u}.\mathbf{u})}{2c_s^2}] \quad (2)$$

where w_α and $\mathbf{e}_\alpha$ quantities are weight factors and discrete velocities, respectively, which are in D2Q9 lattice (see Fig. 1) equal to:

$$\mathbf{e}_\alpha=\begin{cases}0 & ,\ \alpha=0\\ c\left(\cos\theta_\alpha,\sin\theta_\alpha\right) & ,\ \theta_\alpha=(\alpha-1)\pi/2,\ \alpha=1,2,3,4\\ \sqrt{2}c\left(\cos\theta_\alpha,\sin\theta_\alpha\right) & ,\ \theta_\alpha=(\alpha-5)\pi/2+\pi/4,\ \alpha=5,6,7,8\end{cases} \quad (3)$$

$$w_\alpha=\begin{cases}4/9 & ,\ \alpha=0\\ 1/9 & ,\ \alpha=1,2,3,4\\ 1/36 & ,\ \alpha=5,6,7,8\end{cases} \quad (4)$$

By assuming binary flow, the continuity equation can be recast as $\partial\tilde{\rho}_i/\partial t+\nabla\tilde{\rho}_i\mathbf{u}_i=0$, where $\tilde{\rho}_i$ is related to local density and $\mathbf{u}_i$ is velocity of the i-th component (i=1,2). Density $\rho=\sum_{i=1}^{2}\tilde{\rho}_i$ conservation is also observed. In the following, the heavier fluid and the lighter fluid will be distinguished with subscript 1 and 2, respectively. Volume diffusive flow rate $\mathbf{j}_i$ is related to local density and velocity of i-th component by $\rho_i\mathbf{j}_i=\tilde{\rho}_i(\mathbf{u_i}-\mathbf{u})$, where ρ_i is the constant bulk density. By definition of $C=\tilde{\rho}_1/\rho_1$, the continuity equation is rewritten as

$$\partial C/\partial t+\nabla(\mathbf{u}C)=-\nabla\mathbf{j_1} \quad (5)$$

Assuming that the diffusive flow rate depends on the local compositions, it yields $\mathbf{j}_1=-\mathbf{j_2}=\mathbf{j}$ and consequently $\nabla\mathbf{u}=0$. Intermolecular forces are

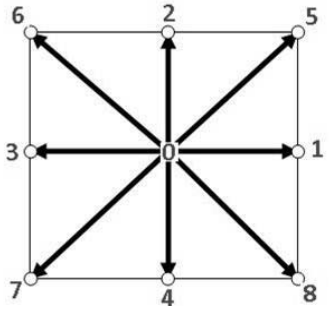

Fig. 1 D2Q9 lattice structure.

also considered as an external force and calculated according to the following equation:

$$\mathbf{F} = \nabla \rho c_s^2 - (\nabla p - C\nabla \mu) \tag{6}$$

where p is related to the dynamic pressure. Also one can take into account the body force effect by adding the following term to Eq. 6:

$$\mathbf{F}_g = \begin{cases} \mathbf{g}(\rho_1 - \rho_2) & , \quad \rho_1 \neq 0, \\ 0 & , \quad \rho_1 = 0, \end{cases} \tag{7}$$

where $\mathbf{F}_g$ is related to gravity, $\mathbf{g}$, ρ_1 and ρ_2 represent the gravitational acceleration, heavy and light densities, respectively. Mixing energy density is estimated using Cahn and Hilliard relation

$$E_{mix}(C, \nabla C) = E_0(C) + \frac{k}{2}\left|\nabla C\right|^2 \tag{8}$$

where k is the gradient parameter and E_0 denotes bulk energy by:

$$E_0(C) \approx \beta C^2 (C-1)^2 \tag{9}$$

where β is a constant. Chemical potential is derived using the following equation:

$$\mu_0 = \frac{\partial E_0}{\partial C} \tag{10}$$

The relation between the gradient parameter, constant parameter β, numerical interface thickness D and the surface tension are given as (Lee, 2009):

$$\kappa = \frac{\beta D^2}{8} \tag{11}$$

$$\sigma = \frac{\sqrt{2\kappa\beta}}{6} \tag{12}$$

Cahn–Hilliard advection equation expresses the diffusive flow rate as a function of chemical potential μ:

$$\mathbf{j} = -M\nabla \mu \tag{13}$$

where $M > 0$ is a constant. Lee (2009), with the definition of another variable, presented his model as follows:

$$g_\alpha = f_\alpha c_s^2 + (p - \rho c_s^2)\Gamma_\alpha(0) \tag{14}$$

Equilibrium distribution function for g_α could be calculated by:

$$g_\alpha^{eq} = f_\alpha^{eq} c_s^2 + (p - \rho c_s^2)\Gamma_\alpha(0) = w_\alpha[p + \rho c_s^2(\frac{\mathbf{e}_\alpha.\mathbf{u}}{c_s^2} + \frac{(\mathbf{e}_\alpha.\mathbf{u})^2}{2c_s^4} - \frac{(\mathbf{u}.\mathbf{u})}{2c_s^2})] \tag{15}$$

In the above equation $\Gamma_\alpha = f_\alpha^{eq} / \rho$.

Material derivative $D_t = \partial_t + \mathbf{e}_\alpha.\nabla$ of g_α is of the form:

$$\frac{\partial g_\alpha}{\partial t} + \mathbf{e}_\alpha.\nabla g_\alpha = -\frac{1}{\lambda}(g_\alpha - g_\alpha^{eq}) + (\mathbf{e}_\alpha - \mathbf{u}).[\nabla \rho c_s^2(\Gamma_\alpha - \Gamma_\alpha(0)) - (C\nabla\mu + \mathbf{F}_{ext})\Gamma_\alpha] \tag{16}$$

Distribution function to compute the value of composition C is defined as $h_\alpha = (C/\rho) f_\alpha$ and its equilibrium state yields $h_\alpha^{eq} = (C/\rho) f_\alpha^{eq}$. Similarly total derivative of h_α is of the form:

$$\frac{\partial h_\alpha}{\partial t} + \mathbf{e}_\alpha.\nabla h_\alpha = \frac{C}{\rho}[-\frac{1}{\lambda}(f_\alpha - f_\alpha^{eq}) + \frac{(\mathbf{e}_\alpha - \mathbf{u}).\mathbf{F}}{c_s^2}\Gamma_\alpha] = -\frac{1}{\lambda}(h_\alpha - h_\alpha^{eq}) + f_\alpha \frac{D}{Dt}(\frac{C}{\rho}) + \frac{C}{\rho c_s^2}(\mathbf{e}_\alpha - \mathbf{u}).[\nabla \rho c_s^2 - (\nabla p + C\nabla\mu + \mathbf{F_{ext}})]\Gamma_\alpha \tag{17}$$

One can estimate

$$f_\alpha \frac{D}{Dt}(\frac{C}{\rho}) \approx (\frac{\partial C}{\partial t} + \mathbf{e}_\alpha.\nabla C)\Gamma_\alpha - \frac{C}{\rho}(\frac{\partial \rho}{\partial t} + \mathbf{e}_\alpha.\nabla\rho)\Gamma_\alpha = [(\mathbf{e}_\alpha - \mathbf{u}).\nabla C + M\nabla^2\mu]\Gamma_\alpha - \frac{C}{\rho}(\mathbf{e}_\alpha - \mathbf{u}).\nabla\rho\Gamma_\alpha \tag{18}$$

Finally by substituting Eq. 18 into Eq. 17, we have

$$\frac{\partial h_\alpha}{\partial t} + \mathbf{e}_\alpha.\nabla h_\alpha = -\frac{1}{\lambda}(h_\alpha - h_\alpha^{eq}) + M\nabla^2\mu\Gamma_\alpha + (\mathbf{e}_\alpha - \mathbf{u}).[\nabla C - \frac{C}{\rho c_s^2}(\nabla p + C\nabla\mu + \mathbf{F_{extt}})]\Gamma_\alpha \tag{19}$$

2.2 Discretization of equations

The discrete form of Eqs. 16 and 19 with respect to the time step δt are summarized as follows:

$$\bar{g}_\alpha(\mathbf{x} + \mathbf{e}_\alpha\delta t, t + \delta t) = \bar{g}_\alpha(\mathbf{x}, t) - \frac{1}{\tau + 0.5}(\bar{g}_\alpha - \bar{g}_\alpha^{eq})(\mathbf{x}, t) + \delta t(\mathbf{e}_\alpha - \mathbf{u}).[\nabla \rho c_s^2(\Gamma_\alpha - \Gamma_\alpha(0)) - C(\nabla\mu + \mathbf{F_{ext}})\Gamma_\alpha]\Big|_{(\mathbf{x},t)} \tag{20}$$

where $\bar{g}_\alpha$ is introduced to summarize equations

$$\bar{g}_\alpha = g_\alpha + \frac{1}{2\tau}(g_\alpha - g_\alpha^{eq}) - \frac{\delta t}{2}(\mathbf{e}_\alpha - \mathbf{u}).[\nabla \rho c_s^2(\Gamma_\alpha - \Gamma_\alpha(0)) - C\nabla\mu\Gamma_\alpha] \quad (21)$$

and

$$\bar{g}_\alpha^{eq} = g_\alpha^{eq} - \frac{\delta t}{2}(\mathbf{e}_\alpha - \mathbf{u}). [\nabla \rho c_s^2(\Gamma_\alpha - \Gamma_\alpha(0)) - C\nabla\mu\Gamma_\alpha] \quad (22)$$

Similarly for $\bar{h}_\alpha$ we have

$$\bar{h}_\alpha(\mathbf{x} + \mathbf{e}_\alpha \delta t, t + \delta t) = \bar{h}_\alpha(\mathbf{x}, t) - \frac{1}{\tau + 0.5}(\bar{h}_\alpha - \bar{h}_\alpha^{eq})(\mathbf{x}, t) + \delta t(\mathbf{e}_\alpha - \mathbf{u}).[\nabla C - \frac{C}{\rho c_s^2}(\nabla p + C\nabla\mu)]\Gamma\big|_{(\mathbf{x},t)} + \delta t \nabla.(M\nabla\mu)\Gamma_\alpha\big|_{(\mathbf{x},t)} \quad (23)$$

where

$$\bar{h}_\alpha = h_\alpha + \frac{1}{2\tau}(h_\alpha - h_\alpha^{eq}) - \frac{\delta t}{2}(\mathbf{e}_\alpha - \mathbf{u}).[\nabla C - \frac{C}{\rho c_s^2}(\nabla p + C\nabla\mu)]\Gamma\big|_{(\mathbf{x},t)} \quad (24)$$

and

$$\bar{h}_\alpha^{eq} = h_\alpha^{eq} - \frac{\delta t}{2}(\mathbf{e}_\alpha - \mathbf{u}).[\nabla C - \frac{C}{\rho c_s^2}(\nabla p + C\nabla\mu)]\Gamma\big|_{(\mathbf{x},t)} \quad (25)$$

Finally the value of compositions, momentum and dynamic pressure are presented, as follows:

$$C = \sum_\alpha \bar{h}_\alpha \quad (26)$$

$$\rho\mathbf{u} = \frac{1}{c_s^2}\sum_\alpha \mathbf{e}_\alpha \bar{g}_\alpha - \frac{\delta t}{2} C\nabla\mu \quad (27)$$

$$p = \sum_\alpha \bar{g}_\alpha + \frac{\delta t}{2}\mathbf{u}.\nabla\rho c_s^2 \quad (28)$$

Density and dimensionless relaxation time variations for two fluids are estimated by linear relation as: $\rho = C\rho_1 + (1-C)\rho_2$ and $\tau = C\tau_1 + (1-C)\tau_2$.

2.3 Contact angle

In order to consider the contact angle effects on droplet dynamics, Cahn's wetting theory is used in solid-fluid interfaces. To guarantee no-mass flux on the solid body, chemical potential gradient in the direction normal to the solid boundary requires:

$$\mathbf{n}.\nabla\mu\big|_w = 0 \quad (29)$$

where $\mathbf{n}$ is the unit vector normal to the surface. Minimization of the total free energy Ψ, with respect to C, neglecting the terms higher than second order in Ψ_s, yields (Lee and Liu, 2010):

$$\vec{n}.\nabla C\big|_w = \sqrt{2\beta/k}\,\Omega_1(C - C^2) \quad (30)$$

By introducing a new non-dimensional parameter as wetting potential $\Omega_1 = \varphi_1/\sqrt{2k\beta}$, one can determine the equilibrium contact angle θ_{eq}:

$$\cos\left(\theta^{eq}\right) = \frac{\sigma_{SG} - \sigma_{SL}}{\sigma} = -\Omega_c \quad (31)$$

In the above equation σ_{SG} denotes surface tension between solid and gas and σ_{Sl} is related to surface tension between solid and liquid. In order to verify the code's accuracy, different equilibrium contact angles were simulated and results compared with Eq. 31. As it is shown in Fig. 2 the agreement is very good. Fig. 3 shows three different equilibrium states in contact angles of 30, 90 and 120 degrees.

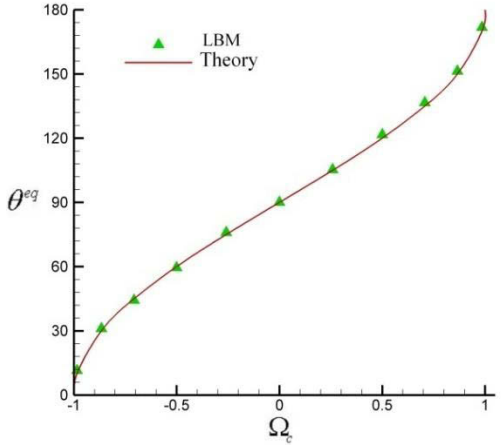

Fig. 2 Comparison between simulated and analytical equilibrium contact angles.

Fig. 3 Three different equilibrium states in contact angle of: (a) 30 degree, (b) 90 degree, and (c) 120 degree.

3. RESULTS AND DISCUSSION

3.1 Problem definition

In this section we deal with the problem of droplet dripping through a hole, under gravity and capillary pressure effects. As our study is implemented in a two-dimensional domain, a droplet will seem to have a cylindrical shape and the hole diameter is replaced by the hole' width. Fig. 4 shows a schematic of this problem.

In this figure, L is the hole's width, D represents the diameter of the droplet, h is the thickness of wall, and H is the distance from the droplet centre to the solid wall. In this simulation, density and dynamic viscosity could be considered consistent with water and vapour saturated at 500℃. Surface tension, gravitational acceleration, viscosity and density ratio and the following dimensionless parameters are involved in this problem:

$h^* = \frac{h}{D}$ (Dimensionless height of the droplet)

$L^* = \frac{L}{D}$ (Dimensionless width of the hole)

Throughout the calculations, the density ratio is fixed at 100, and the initial velocity is set to zero. Dimensionless time is utilized to report the results, given by:

$$t^* = \frac{T}{t_h} \tag{32}$$

where T stands for the product of the number of iterations and dt(=1s) and t_h is the characteristic time defined as follows:

$$t_h = \frac{\rho_l^{sat} v_l^{sat} R}{\sigma} \tag{33}$$

where R is the droplet radius, ρ_l^{sat} is the saturated liquid density and v_l^{sat} expresses the kinematic viscosity of saturated liquid and.

The influence of gravitational acceleration measured by Archimedes number is defined as follows:

$$Ar = \frac{\rho_l \sqrt{gD^3}}{\mu_l} \tag{34}$$

where D and g are initial droplet diameter and gravitational acceleration, respectively. And the effect of surface tension is measured by Ohnesorge number:

$$Oh = \frac{\mu_l}{\sqrt{\rho_l D \sigma}} \tag{35}$$

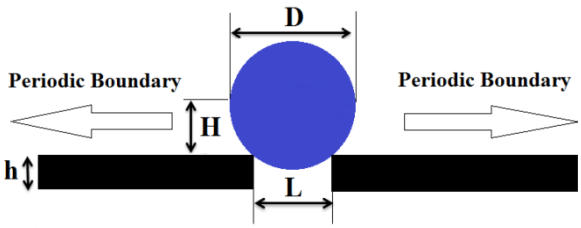

Fig. 4 Schematic of problem.

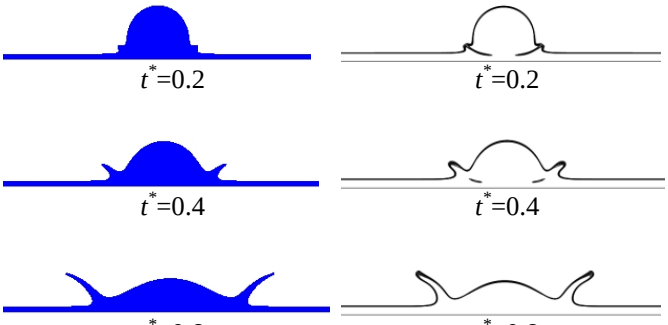

Fig. 5 Droplet splashing on thin liquid film, *Re*=500, *We*=8000 and *h** =0.15: (a) current simulation; (b) results of Lee and Lin (2005).

In order to verify code accuracy in two-phase modelling, droplet splashing on a thin liquid film test was performed and its results were compared with Lee's work (Lee, 2005). For this reason some non-dimensional parameters, such as Reynolds number $Re = \rho_1 U_0 D / \mu_1$, Weber number $We = \rho_1 U_0{}^2 D / \sigma$ and non-dimensional height of liquid film $h^* = h / D$ are used, where h is liquid film height on the surface and D represents the droplet diameter and subscript 1 stands for droplet. Numerical results of *Re*=500, *We*=8000 and h^* =0.15 are shown in Fig. 5. Comparison of current work results with those of Lee and Lin (2005) shows the two-phase code accuracy.

3.2 Grid resolution dependence

The computational domain is divided into 200×100, 400×200 and 600×300 lattices for three simulations. Fig. 6 confirms that the grid resolution has no substantial effect on the results. So to prevent high computational cost, the grid 400×200 for all simulation was used.

3.3 Contact angle effect

Before study of the main issue, in this section we investigate the equilibrium contact angle behaviour. For this reason the spread factor

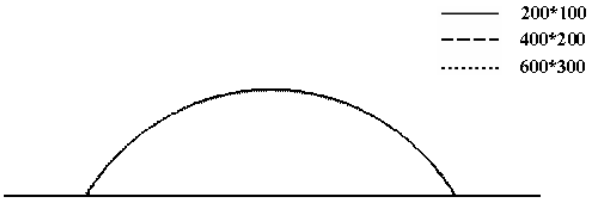

Fig. 6 Grid resolution of droplet formation on solid surface.

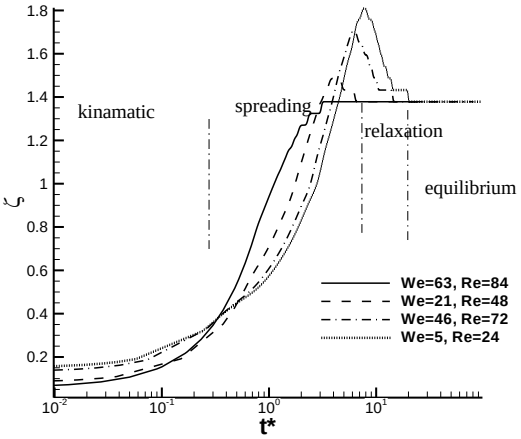

Fig. 7 Spread factor variation of droplet after hitting the surface, *Oh*=0.0943.

$\zeta = d/D$ is defined as a ratio of wetted diameter on the solid surface to initial diameter of the droplet. We put the density ratio, dynamic viscosity ratio and equilibrium contact angle equal to 100, 10 and 90 degrees, respectively. Droplet behaviour after its collision with solid surface is plotted in Fig. 7 in different Reynolds and Weber numbers when its Ohnesorge number is equal to 0.0943. In this figure four phases appear when the droplet collides with solid surface: kinematic, spreading, relaxation and equilibrium phases. According to Fig. 7, the spread factor is a function of the Reynolds and Weber numbers which control the required time for reaching equilibrium condition. With increasing Weber number, the droplet spreading on the surface (wetted diameter) will increase, which lengthens the equilibrium process.

When the Weber number becomes less than 5, droplet collision has no relaxation phase and reaches its equilibrium state after spreading phase. Gupta and Kumar (2011) have proposed the equation of $\zeta = 1.42\sqrt{t^*}$ in kinematic phase. Fig. 8 shows the spread factor variation versus t^* for different Reynolds and Weber numbers. From this figure a good agreement can be seen between current work and given correlation.

In the following part of this section we will examine the droplet behavior dripping down a

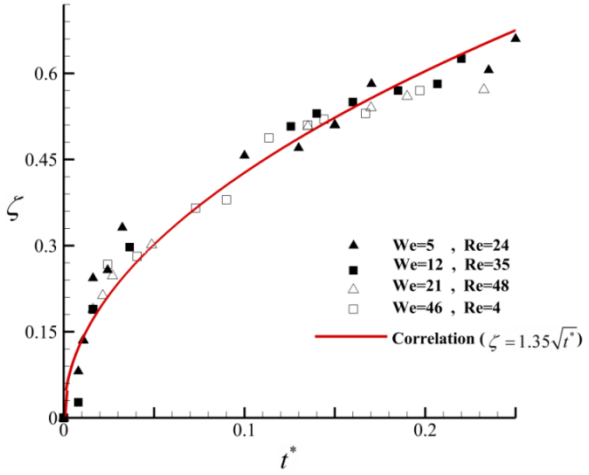

Fig. 8 Spread factor variation of droplet after hitting surface at kinematic phase, *Oh*=0.0943.

hole for three equilibrium contact angles of 60, 90 and 120 degrees. It is expected that for contact angles less than 90 degrees the surface will be hydrophilic and some parts of the droplet tends to stay on the surface. As can be seen in Fig. 9a, for the equilibrium contact angle of 60° with hydrophilic behaviour of the droplet on the surface, it is pulled along the horizontal axis. Simultaneously the central part of the droplet, which is in line with the hole, moves downward under its gravity into the hole.

Since surface tension in the central part of the droplet cannot overcome the shear forces on the surface and the droplet inertia, hence droplet decays and parts of it remain on the surface. Also at the contact angle of 90 degrees the surface tension, which imposes itself into the middle part of the droplet, cannot overcome inertia force. This causes the remote parts of the droplet to remain stationary so that the middle part of the droplet will separate from the two ends on the surface. As shown in Fig. 9b, the droplet volume which remains on the surface is less than the last one with a lower contact angle. For a contact angle of 120 degrees, the surface can be considered hydrophobic and the droplet spread will decrease on the surface. This makes it possible for the surface tension to overcome the inertia force, and so the droplet passes through the hole totally. Therefore, by increasing equilibrium contact angle, the droplet tendency for remaining on the surface decreases.

3.4 Surface tension and gravity effects

In order to investigate the effects of surface tension on the droplet dynamics, all of the parameters involved in the problem have been fixed and only the surface tension changes. All

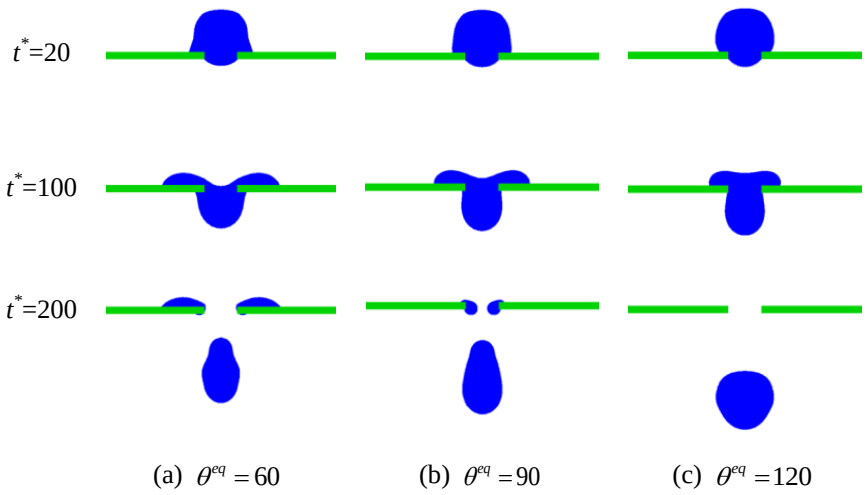

Fig. 9 Droplet deformation under gravity obtained at kinematic viscosity ratio of 25, density ratio of 100 (*Ar*=79.06 *Oh*=0.032).

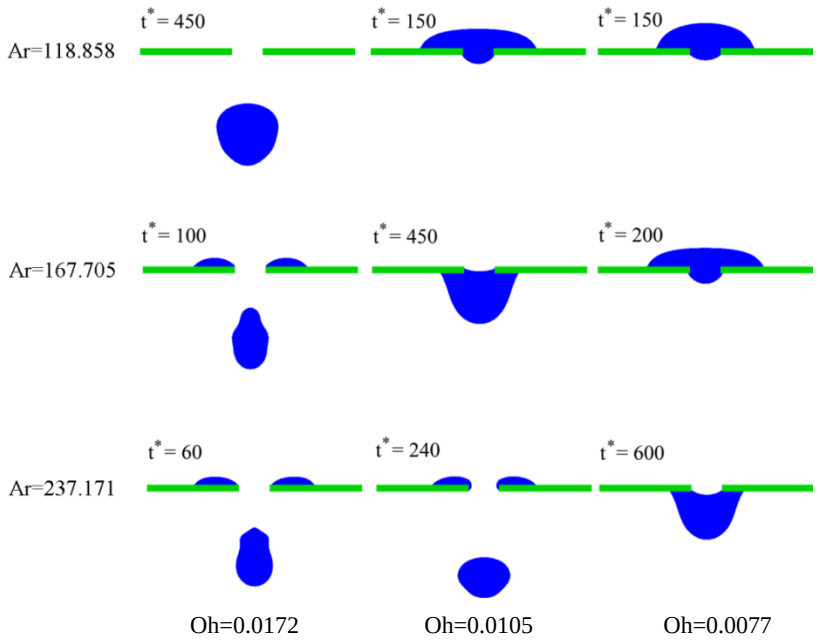

Fig. 10 Droplet deformation under influence of surface tension and gravity changes at equilibrium angle of 60 degrees.

results in this section are related to density ratio of 100, kinematic viscosity ratio of 10 and the contact angle set to 60 degrees. Also, to investigate the gravitational effects, all other parameters are held fixed and only the acceleration of gravity (g) is changed. The results of the surface tension and gravity effects are shown in Fig. 10. In this figure, gravity increases from top to bottom and surface tension from left to right, as gravity increases the surface tension also increases. As can be seen in Fig. 10, at any given Ohnesorge number, by increasing the Archimedes number (by increasing the gravitational acceleration) the droplet has greater tendency to pass through the hole. With decreasing Ohnesorge number (by increasing the surface tension), however, the droplet tends to retain its state and resists against the gravitational force. Note that the presented times are in different values because of different times required for droplet to reach stable conditions in different conditions. At *Oh*=0.0172 with increasing *Ar*, droplet accelerates in passing the hole. While the remote parts of the droplet on the surface (which are influenced by surface force) does not have enough time to overcome this force hence decays to some small parts (*Oh*=0.0172 and *Ar*=167.705). For the case of *Oh*=0.0105 and *Ar*=118.585, surface tension forces are dominant and the droplet tends to keep its initial shape thus

equilibrium is reached after passing a bit through the hole. By increasing the Archimedes number to 167.705 by the increase of gravitational force, the droplet passes the hole totally but it cannot drip from the bottom of the surface. If gravity is large enough (*Ar*=237.171) a part of the droplet remains on the upper surface and the residual droplet passes through the hole and falls down. For different values of surface tension, gravity, and equilibrium contact angle, the final states of the droplet are divided into four categories, the balance of the droplet at the top, the balance at the bottom, decay, and droplet falling.

3.5 Effect of width ratio and dimensionless height of hole

In order to investigate the effect of width and height ratio of the hole on droplet behaviour, all parameters were held constant except width and height of the hole. Fig. 11 illustrates this effect. As can be seen in this figure, with increasing height and decreasing width of the hole, shear forces on the solid surface become stronger. This force is a resistance force against the weight of the droplet. Therefore increasing shear forces causes reduction in flow rate and decay of the droplet takes longer time. Note that any increase in the width of the hole can diminish the effect of an increase in the droplet height.

3.6 Density ratio effect

To consider the effect of the density ratio on the droplet dynamics, three different density ratios of 10, 100 and 500 for given time and other parameters shown in Fig. 12 have been considered. From this figure, very little differences in the effects of density ratios of 100 and 500 can be seen, so the results can be considered to be virtually the same. Since gravity will exert itself as a buoyant force (Bower and Lee, 2010), any increase in density ratio will amplify the buoyancy force and a larger force will act on the droplet. This causes more displacement compared with low density ratios.

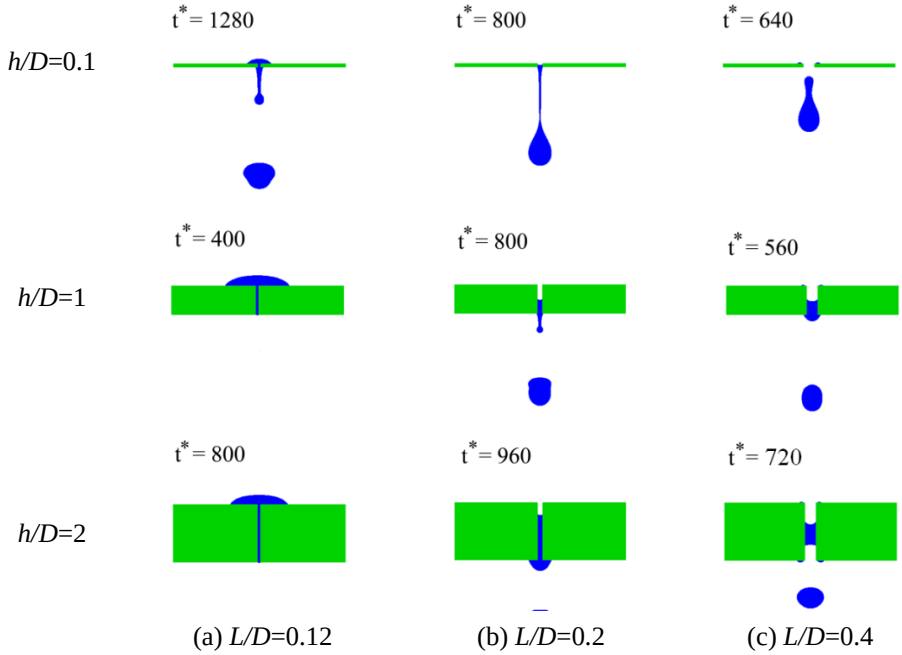

Fig. 11 Effects of dimensionless width and height of hole on droplet behavior ($\theta^{eq} = 60$, *Ar*=79.06 and *Oh*=0.032).

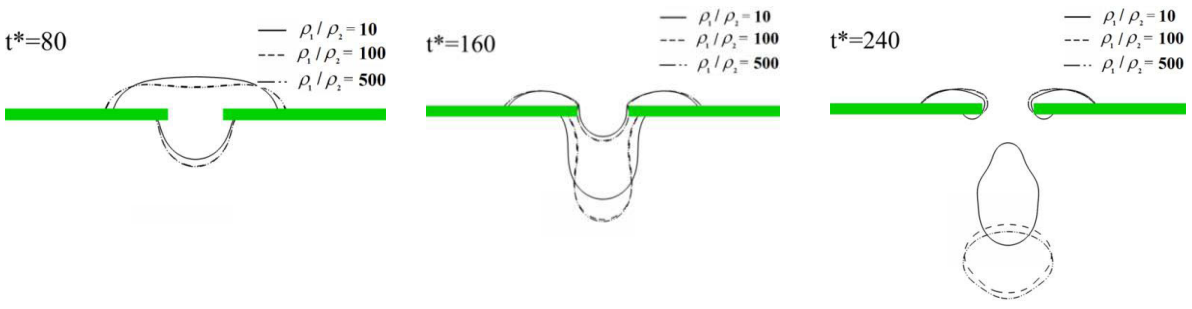

Fig. 12 Effect of density ratio on droplet shape in kinematic viscosity ratio of 1 ($\theta^{eq} = 60$, *Ar*=236 and *Oh*=0.011).

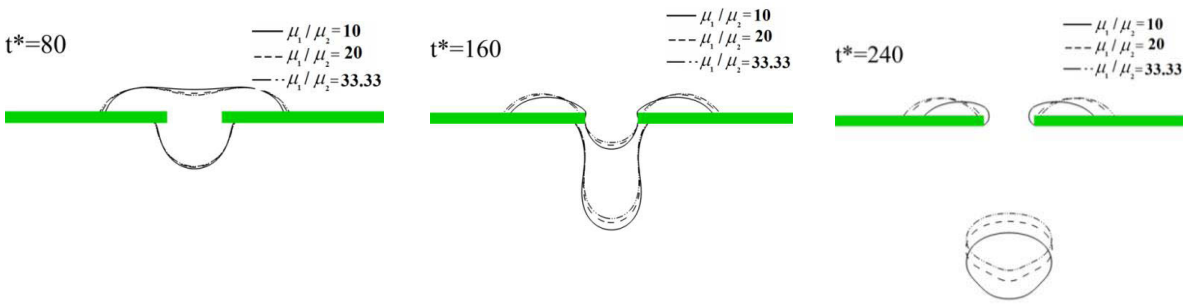

Fig. 13 Effect of dynamic viscosity ratio on droplet deformation with density ratio of 100 ($\theta^{eq} = 60$, *Ar*=236 and *Oh*=0.011).

3.7 Viscosity ratio effect

To consider the effect of the dynamic viscosity on droplet dynamics, three dynamic viscosity ratios of 10, 20 and 33.33 have been simulated. The results are shown in Fig. 13. It needs to be mentioned that, in practice, the dynamic viscosity of the liquid was fixed and the dynamic viscosity ratio was increased by reducing the viscosity of the gas phase. As expected, decrease in the dynamic viscosity of the gas decreases the resistance against the droplet deformation. Fig. 13 shows droplet deformation with viscosity ratio variation in three different points of times.

4. CONCLUSIONS

Lattice Boltzmann method was used to simulate droplet motion through a hole located on a horizontal surface. For this reason, Lee's LBM model with consideration of the liquid-solid contact angle effect was studied and the effects of different parameters were investigated. Besides the numerical results, high stability in the two-phase modelling, especially in capturing the remaining fine particles on the surface and slender strip of droplet which is passing through the small hole, and capability of the method in controlling the surface tension and contact angle fascinated the authors to model this problem. Results have shown that by increasing equilibrium contact angle, the droplet tendency for remaining on the surface decreases. Also any increase in the Archimedes number magnifies the droplet tendency to pass through the hole. Moreover decreasing the Ohnesorge number increases the droplet tendency to retain its state and resists against the gravitational force. The effect of height and width of the hole on the droplet behaviour is such that by increasing the height and decreasing the width of the hole, the shear force on the solid surface becomes stronger and leads to reduction in flow rate and decay of the droplet takes longer time. Also the effect of increasing the height of hole can be weakened by reducing the hole'swidth. Simulation results have confirmed that increasing the density ratio will amplify the buoyancy force and consequently a larger force will act on the droplet. This causes more displacement compared with low density ratios. Furthermore increasing the viscosity ratio does not have considerable effect on droplet deformation. Finally based on the results obtained in this work, four different states have been distinguished: equilibrium on the upper surface, equilibrium on the bottom surface, and decay and dripping of the droplet. It should also be noted that the current study solved a two-dimensional problem and its results are related to a two-dimensional droplet which may deviate from those of a physical 3D problem. The current study should be extended to 3D domain in future works.

REFERENCES

1. Bower LA, Lee T (2010). Single bubble rising dynamics for moderate Reynolds number using Lattice Boltzmann method. *Computers and Fluid* 39:1191-1
2. Briant AJ, Papatzacos P, Yeomans JM (2002). Lattice Boltzmann simulations of contact line motion in a liquid-gas system. *Phil. Trans. R. Soc. Lond. A.* 360:485-495.
3. Briant AJ, Wagner AJ, Yeomans JM (2004). Lattice Boltzmann simulations of contact line motion. I. Liquid-gas systems. *Phys. Rev. E* 69:031602.
4. Castanet G, Liénart T, Lemoine F (2009). Dynamics and temperature of droplets impacting onto a heated wall. *International Journal of Heat and Mass Transfer* 52:670-679.
5. Chen S, Doolen GD (1998). Lattice Boltzmann method for fluid flows. *Annu. Rev. Fluid Mech* 30:329-364.
6. Connington K, Lee T (2012). A review of spurious currents in the lattice Boltzmann

method for multiphase flows. *J Mech Sci Technol*. 26(12):3857-3863.
7. Cossali GE, Marengo M, Coghe A, Zhdanov S (2004). The role of time in single droplet splash on thin film. *Experiments in Fluids* 36:888-900.
8. Ghosh S, Patil P, Mishra SC, Das AK, Das PK (2012). 3-D lattice Boltzmann model for asymmetric taylor bubble and taylor droplet in inclined channel. *Engineering Applications of Computational Fluid Mechanics* 6(3):383-349.
9. Gupta A, Kumar R (2011). Tow-dimensional lattice Boltzmann model for droplet impingement and breakup in low density ratio liquids. *Commun. Comput. Phys* 10(3):767-784.
10.
11. He X, Shan X, Doolen GD (1998). A discrete Boltzmann equation model for non-ideal gases. *Phys. Rev. E* 57:R13.
12. Inamuro T, Ogata T, Tajima T, Konishi N (2004). A lattice Boltzmann method for incompressible two-phase flows with large density differences. *J. Comput. Phys* 198:628-644.
13. Krause F, Li X, Fritsching U (2011). Simulation of droplet-formation and –interaction in emulsification processes. *Engineering Applications of Computational Fluid Mechanics* 5(3):406-415.
14. Kupershtok L, Medvedev DA, Karpov DI (2009). On equations of state in a lattice Boltzmann method. *Comput. Math. Appl.* 58:965-974.
15. Lee T (2009). Effects of incompressibility on the elimination of parasitic currents in the lattice Boltzmann equation method for binary fluids. *Comput. Math. Appl.* 58:987-994.
16. Lee T, Lin CL (2005). A stable discretization of the lattice Boltzmann equation for simulation of incompressible two-phase flows at high density ratio. *J. Comput. Phys.* 206:16-47.
17. Lee T , Liu L (2010). Lattice Boltzmann simulations of micron-scale droplet impact on dry surfaces. *J. Comput. Phys* 229:8045-8063.
18. Lunkad SF, Buwa VV, Nigam KDP (2007). Numerical simulations of droplet impact and spreading on horizontal and inclined surfaces. *Chem. Eng. Sci* 62:7214-7224.
19. Manservisi S, Scardovelli R (2009). A variational approach to the contact angle dynamics of spreading droplets. *Comput. Fluids* 38:406-424.
20. Pan KL, Law CK (2007). Dynamics of droplet–film collision. *J. Fluid Mech* 587:1-22.
21. Succi S (2001). *The Lattice Boltzmann Equation for Fluid Dynamics and Beyond*. Oxford: Clarendon Press.
22. Taghilou M, Rahimian MH (2012). Investigation of two phase flow in porous media using lattice Boltzmann Lee method. *9th International Conference for Mesoscopic Methods in Engineering and Science*, Taipei, Taiwan.
23. Wal RLV, Berger GM, Mones SD (2006). Droplets splashing upon films of the same fluid of various depths. *Experiments in Fluids* 40:33-52.
24. Yoshino M, Mizutani Y (2006). Lattice Boltzmann simulation of liquid-gas flows through solid bodies in a square duct. *Math. Comput. Simul.* 72:264-9.